

SPECTRA AND DIAGNOSTICS FOR THE DIRECT DETECTION OF WIDE-SEPARATION EXTRASOLAR GIANT PLANETS

ADAM BURROWS¹, DAVID SUDARSKY¹, & IVAN HUBENY^{1,2,3}
Draft version August 29, 2018

ABSTRACT

We calculate as a function of orbital distance, mass, and age the theoretical spectra and orbit-averaged planet/star flux ratios for representative wide-separation extrasolar giant planets (EGPs) in the optical, near-infrared, and mid-infrared. Stellar irradiation of the planet's atmosphere and the effects of water and ammonia clouds are incorporated and handled in a consistent fashion. We include predictions for 12 specific known EGPs. In the process, we derive physical diagnostics that can inform the direct EGP detection and remote sensing programs now being planned or proposed. Furthermore, we calculate the effects of irradiation on the spectra of a representative companion brown dwarf as a function of orbital distance.

Subject headings: planetary systems—binaries: general—planets and satellites: general—stars: low-mass, brown dwarfs—radiative transfer—molecular processes—infrared: stars

1. INTRODUCTION

To date, more than 110 EGPs (Extrasolar Giant Planets) have been discovered by the radial-velocity technique around stars with spectral types from M4 to F7⁴. A sample of relevant references to the discovery literature, by no means exhaustive, includes Mayor and Queloz (1995), Marcy and Butler (1996), Butler et al. (1997,1999), Marcy et al. (1998,1999), Marcy, Cochran, and Mayor (2000), Queloz et al. (2000), Santos et al. (2000), and Konacki et al. (2003). These planets have minimum masses ($m_p \sin(i)$, where i is the orbital inclination) between $\sim 0.12 M_J$ and $\sim 15 M_J$ ($M_J \equiv$ one Jupiter mass), orbital semi-major axes from ~ 0.0225 AU to ~ 5.9 AU, and eccentricities from ~ 0 to above 0.7. Given our all-too-narrow experience within the solar system, such variety and breadth was wholly unanticipated.

Importantly, two EGPs (HD 209458b and OGLE-TR-56b) have been found to transit their primaries (Henry et al. 2000; Charbonneau et al. 2000,2001; Brown et al. 2001; Konacki et al. 2003; Torres et al. 2003). Furthermore, in the first measurement of the composition of an extrasolar planet of any kind, Charbonneau et al. (2002) detected sodium (Na-D) in their HD 209458b transit spectrum. This was followed by the detection of atomic hydrogen at Lyman- α and the discovery of a planetary wind (Vidal-Madjar et al. 2003; Burrows and Lunine 1995). With both transit and radial-velocity data, an EGP's mass and radius can be determined, enabling its physical and structural study. Such data can resolve the ambiguity inherent in the radial-velocity technique's sensitivity to only the combination $m_p \sin(i)$. Precision astrometry can also be used to derive masses, as has been done for GJ 876b with the Fine Guidance Sensors on HST (Bennett et al. 2002), and space interferometry using SIM (Unwin and Shao 2000) promises to provide unprecedented astrometric masses by the year ~ 2010 .

However, it is only by direct detection of a planet's light using photometry, spectrophotometry, or spectroscopy that the detailed and rigorous study of its physical attributes can be conducted. By this means, the composition, gravity, radius, and mass of the giant might be derived and the general theory of

EGP properties and evolution might be tested (Burrows et al. 1995,1997; Marley et al. 1999; Sudarsky, Burrows and Pinto 2000; Sudarsky, Burrows, and Hubeny 2003 (SBH); Baraffe et al. 2003). For close-in EGPs, we can anticipate in the next few years wide-band precision photometry from MOST (Matthews et al. 2001), Kepler (Koch et al. 1998), Corot (Antonello and Ruiz 2002), or MONS (Christensen-Dalsgaard 2000) that will provide the variations of the summed light of the planet and star due to changes in the planetary phase. In the mid- to far-infrared, the Spitzer Space Telescope (a.k.a. SIRTf, Space InfraRed Telescope Facility; Werner and Fanson 1995) might soon be able to measure the variations in the planet/star flux ratios of close-in EGPs (SBH). For wide-separation EGPs, it is necessary to measure the planet's light from under the glare of the primary star at very high star-to-planet contrast ratios. To achieve this from the ground, telescopes such as the VLT interferometer (Paresce 2001), the Keck interferometer (van Belle and Vasisht 1998; Akeson and Swain 2000; Akeson, Swain, and Colavita 2001), and the LBT nulling interferometer (Hinz 2001) will be enlisted. From space, the Terrestrial Planet Finder (TPF, Levine et al. 2003) and/or a coronagraphic optical imager such as *Eclipse* (Trauger et al. 2000,2001) could obtain low-resolution spectra.

To support the above efforts and planning for future programs of direct detection of extrasolar giant planets and to provide the theoretical context for the general analysis of the spectra and photometry of irradiated and isolated EGPs, our group has embarked upon a series of papers of EGP spectra, evolution, chemistry, transits, orbital phase functions, and light curves. The most recent paper in this series (SBH) explored generic features of irradiated EGP spectra as a function of orbital distance, cloud properties, and composition class (Sudarsky, Burrows, and Pinto 2000). Our technical approach vis à vis radiative transfer, molecular abundance determinations, and cloud modeling is described in detail in that paper, to which the interested reader is referred. However, SBH did not explore the diagnostics of planetary mass and age. In addition, in their study of the orbital distance dependence of EGP spectra SBH did not

¹ Department of Astronomy and Steward Observatory, The University of Arizona, Tucson, AZ 85721

² NOAO, Tucson, AZ 85726

³ NASA Goddard Space Flight Center, Greenbelt, MD 20771

⁴ see J. Schneider's Extrasolar Planet Encyclopaedia at <http://www.obspm.fr/encycl/encycl.html> for a reasonable listing, with comments.

incorporate the effects of water or ammonia clouds in a fully consistent fashion.

In the current paper, we allow our atmosphere code to determine cloud placement in a fully iterative, converged fashion. The result is a consistent determination of the dependence on distance of the spectra of EGPs irradiated by a G2V star, including the effects of the water and ammonia clouds that should form in their atmospheres. In §2, we summarize our numerical approach. Then in §3 we present and describe our results for the dependence of the spectra of irradiated EGPs on orbital distance. In this paper, we emphasize the results for EGPs at wider separations (> 0.2 AU) and defer discussion of the corresponding theory for close-in EGPs to a later paper⁵. This section treats the entire expected range of EGP emission/reflection spectra and behavior. In §4, we provide a representative sequence of models that portray the dependence of irradiated EGP spectra on age, at a given mass and orbital distance. In §5, we present a representative sequence with EGP mass, at a given age and orbital distance. Section 6 is a digression into the effect of stellar irradiation on companion brown dwarfs, characterized by much larger masses and more slowly decaying heat content. We study the signature in the optical of the reflection of stellar light from a companion brown dwarf. In fact, much of this paper is concerned with the signatures and diagnostics of the physical parameters of irradiated substellar-mass companions⁶. However, it is not feasible in one paper to explore all the possible combinations of planetary mass, age, composition, orbital semi-major axis, eccentricity, and orbital phase with all stellar types. Hence, to maintain a reasonable focus, we restrict our discussions to G2V primaries, zero eccentricity orbits, and solar metallicity. We narrow our scope further by plotting only phase-averaged spectra (as in SBH) at zero orbital inclination. Papers on EGP orbital phase functions, albedos, and light curves are to follow this one (e.g., Sudarsky, Burrows, and Hubeny 2004). These papers address the dependence on phase and Keplerian parameters. Finally, in §7 we present predicted phase-averaged planet/star flux ratios for several known EGPs at wide separations and §8 reprises the essential conclusions of the paper.

2. NUMERICAL ISSUES

To calculate radiative/convective equilibrium atmospheres and spectra we use a specific variant of the computer program TLUSTY (Hubeny 1988; Hubeny & Lanz 1995). This variant involves the hybrid Complete Linearization/Accelerated Lambda Iteration (CL/ALI) method, although in the present runs we use a full ALI mode which leads to an essential saving of computer time without slowing down the iteration process significantly. In addition, we employ TLUSTY's Discontinuous Finite Element (DFE) version (Castor, Dykema, & Klein 1992). The DFE technique, being first order, is optimal for handling irradiated atmospheres (SBH). All models are converged to one part in 10^3 . Stellar spectra from Kurucz (1994) are used for the incoming fluxes at the outer boundaries. The inner boundary condition is the interior flux and this (indexed by T_{eff}) is taken from the evolutionary models of Burrows et al. (1997) for the given mass and age, unless otherwise indicated. This approximate procedure works well for wider-separation EGPs, but not as well for the closer-in EGPs (< 0.15 AU). We use a standard

mixing-length prescription to handle convection and a mixing length of one pressure scale height. Since the atmosphere code is planar, we use the redistribution technique described in SBH, i.e. we weight the incident flux by 1/2 to account for the average inclination of the planetary surface to the line of sight to the primary. As described in SBH, the planetary spectra we present here are phase/time-averaged over the orbit. Care is taken with this procedure to ensure that energy is conserved and that energy *in* (from the star and the planetary interior) equals energy *out*. To account for the anisotropy of single scattering off of cloud particles, we calculate using Mie theory the average of the cosine of the scattering angle, and reduce the Mie-theory-derived total scattering cross section by one minus this average. With this procedure, we are substituting the "transport cross section" for the total scattering cross section. This approach has been shown to mimic the effect of asymmetric scattering quite well (Sudarsky, Burrows, and Pinto 2000).

For molecular and atomic compositions, we use an updated version of the chemical code of Burrows and Sharp (1999), which includes a prescription to account for the rainout of condensed species in a gravitational field and new thermochemical data. The derived molecular abundances are very similar to those obtained by Lodders (1999) and Lodders and Fegley (2002). Our solar metallicity is defined as the elemental abundance pattern found in Anders and Grevesse (1989). For molecular and atomic opacities, we have developed an extensive database, described in part in Burrows et al. (2001) and SBH.

The treatment of H_2O and NH_3 clouds is done in a manner consistent with their respective condensation curves and the cloud base is put at the intersection of the corresponding condensation curve at solar metallicity with the object's temperature/pressure (T/P) profile. In each iteration of the global ALI scheme, we find a position of the cloud base as the intersection of the corresponding condensation curve with the current T/P profile. The scale height of a cloud is assumed to be equal to one pressure scale height. We use Mie theory for the absorptive and scattering opacities of particles whose model size is determined by the theory of Cooper et al. (2003). In the subsequent iteration of the ALI scheme, we employ this cloud opacity and scattering self-consistently in the radiative transfer equation and the energy balance equation. In the next ALI iteration we again recalculate the position of the cloud base, and the whole process is repeated until the cloud position is fully stabilized. We note that in the initial stages of the global iteration process the cloud position may vary significantly; in some case clouds appear (disappear) after several iterations of the cloudless (cloudy) atmosphere. This procedure ensures that the cloud position is self-consistent with the overall model atmosphere. This also means that the predicted cloud properties, in particular optical depths and base pressures, vary in a physical and consistent way with the orbital distance, mass, and age.

3. ORBITAL DISTANCE DEPENDENCE OF EGP SPECTRA FROM 0.2 TO 15 AU

Figure 1 shows the T/P profiles for the distance sequence from 0.2 to 15 AU for a $1-M_J$ EGP irradiated by a G2V star. For specificity, we have assumed a radius of $1 R_J$ and an internal flux T_{eff} of 100 K for the entire family. According to the models of

⁵ Note, however, that the spectra of close-in EGPs has been addressed in SBH, as well as in Seager and Sasselov (1998,2000), Seager, Whitney, and Sasselov (2000), and Goukenleuque et al. 2000.

⁶ We refer to Substellar-Mass Objects as SMOs.

Burrows et al. (1997), this corresponds roughly to an age of 5 Gyr, but after ~ 0.1 Gyr, the radius and gravity of the EGP vary little. The orbits are taken to be circular, so there is no assumed orbital phase dependence⁷. The intercepts with the dashed lines identified by either $\{\text{NH}_3\}$ or $\{\text{H}_2\text{O}\}$ denote the positions where the corresponding clouds form. Due to the cold trap effect and depletion due to rainout (Burrows and Sharp 1999), the higher-pressure intercept is taken to be at the base of the cloud. The spectral/atmospheric models include the effects of these clouds in a consistent way. Table 1 gives the modal particle sizes in microns that we derive using the theory of Cooper et al. (2003) when a cloud of either water or ammonia (or both) appears. For the ammonia clouds that form in this orbital distance sequence (at $\gtrsim 6$ AU), the modal particle sizes we find hover near $50\text{--}60 \mu\text{m}$. The corresponding particle sizes in the water clouds are near $110 \mu\text{m}$. These particles are larger than for more massive SMOs. Furthermore, we assume that the particle size does not vary with altitude and that the particle size distribution (given a modal radius) is that of Deirmendjian (1964,1969). Clearly, a major ambiguity in EGP modeling is cloud physics (SBH). We have settled on the Cooper et al. (2003) theory to provide a consistent framework.

When the chemistry indicates that both cloud types are present, we include them both in the atmospheric/spectral calculation. As Fig. 1 shows, the ammonia cloud is always above the water cloud. Water clouds form around a G2V star exterior to a distance near 1.5 AU, whereas ammonia clouds form around such a star exterior to a distance near 4.5 AU. Note that Jupiter itself is at the distance from the Sun of ~ 5.2 AU. For the closer-in objects, the T/P profile manifests an inflection. This inflection is a consequence of the dominance of external radiation over the internal heat flux. For longer ages and low masses, the orbital distance at which one must place the SMO/EGP to erase this inflection is large. For this model set, that distance is ~ 2 AU. For larger masses, dimmer primaries, and shorter ages, that distance decreases. In addition, the strong irradiation that produces the inflection in the T/P profile also forces the radiative/convective boundary to recede to higher pressures. For a $1-M_J$ EGP at an orbital distance of 0.05 AU (not shown) around a G2V star, this pressure can be greater than 1000 bars! Such is the case for HD 209458b and OGLE-TR56b (Burrows, Sudarsky, and Hubbard 2003; Fortney et al. 2003).

For comparison, and in anticipation of the discussion in §4 concerning the age dependence of irradiated EGP spectra, Fig. 2 portrays the evolution in the T/P profile of a $1-M_J$ EGP at a distance of 4 AU around a G2V star. Table 2 gives the corresponding modal particle sizes in microns (Cooper et al. 2003) for the ice particles of the water clouds that appear in this evolutionary sequence, as well as the inner flux T_{eff} , gravity, and planet radius as this $1-M_J$ EGP evolves according to the theory of Burrows et al. (1997). The modal particle size is very roughly constant with age. The radius of the $1-M_J$ EGP decreases by $\sim 15\%$ from 0.1 to 5 Gyr. Not surprisingly, at a distance of 4 AU no inflection in the T/P profile is produced. Note that at this orbital distance and as early as ~ 50 Myr (not shown), water clouds form in Jovian-mass objects. Note also that at 4 AU, even after 5 Gyr ammonia clouds have not yet formed in the atmosphere of an irradiated $1-M_J$ EGP. This is not true for a similar object in isolation (Burrows, Sudarsky, and Lunine 2003).

Figure 3 depicts the planet-to-star flux ratios from $0.5 \mu\text{m}$ to

$30 \mu\text{m}$ for the orbital distance study associated with the T/P profiles shown in Fig. 1. In the optical, the flux ratios vary between 10^{-8} and 10^{-10} . In the near infrared, this ratio varies widely from $\sim 10^{-4}$ to 10^{-16} . However, in the mid-infrared beyond $10 \mu\text{m}$, the flux ratio varies more narrowly from 10^{-4} to 10^{-7} . Hence, it makes a difference in what wavelength region one conducts a search for direct planetary light.

Gaseous water absorption features (for all orbits) and methane absorption features (for the outer orbits) sculpt the spectra. The reflected component due to Rayleigh scattering and clouds (when present) is most manifest in the optical and the emission component (similar to the spectrum of an isolated low-gravity brown dwarf) takes over at longer wavelengths. For the EGPs interior to ~ 1.0 AU, the fluxes longward of $\sim 0.8 \mu\text{m}$ are primarily due to thermal emission, not reflection. These atmospheres do not contain condensates and are heated efficiently by stellar irradiation. As a result, the Z ($\sim 1.0 \mu\text{m}$), J ($\sim 1.2 \mu\text{m}$), H ($\sim 1.6 \mu\text{m}$), and K ($\sim 2.2 \mu\text{m}$) band fluxes are larger by up to several orders of magnitude than those of the more distant EGPs. Generally, clouds increase a planet's flux in the optical, while decreasing it in the J , K , L' ($\sim 3.5 \mu\text{m}$), and M ($\sim 5.0 \mu\text{m}$) bands. The transition between the reflection and emission components moves to longer wavelengths with increasing distance, and is around $0.8\text{--}1.0 \mu\text{m}$ at 0.2 AU and $\sim 3.0 \mu\text{m}$ at 15 AU. However, since the irradiation and atmospheric structure and spectra are being calculated self-consistently, emission and reflection components are in fact inextricably intertwined and it is not conceptually correct to separate them.

At large distances exterior to ~ 3.5 AU, the flux longward of $\sim 15 \mu\text{m}$ manifests undulations due to pressure-induced absorption by H_2 . Importantly, there is always a significant bump around the M band at $4\text{--}5 \mu\text{m}$. The peak of this bump shifts from $\sim 4 \mu\text{m}$ to $\sim 5 \mu\text{m}$ with increasing orbital distance. Though muted by the presence of clouds, it is always a prominent feature of irradiated EGPs, as it is in T dwarfs and the Jovian planets of our solar system. Curiously, but not unexpectedly, as Fig. 3 indicates, the planet/star flux ratio is most favorable in the mid-infrared. This fact should be of some interest to those planning TPF or successor missions to the Spitzer Space Telescope.

Though the major trend is a monotonic decrease in a planet's flux with increasing orbital distance, the 0.2-AU model atmosphere is hot enough that the sodium and potassium resonance absorption lines appear and suppress the flux around Na-D ($0.589 \mu\text{m}$) and the related K I doublet at $0.77 \mu\text{m}$. The result is a lower integrated visible flux that is comparable to that of the otherwise dimmer 0.5-AU model. Figures 4 and 5 focus in on the $0.5 \mu\text{m}$ to $2.0 \mu\text{m}$ region and allow one to distinguish one model from another at shorter wavelengths more easily than is possible in the panoramic Fig. 3. These figures allow us to see that for greater orbital distances, the atmospheric temperatures are too low for the alkali metals to appear, but the methane features near $0.62 \mu\text{m}$, $0.74 \mu\text{m}$, $0.81 \mu\text{m}$, and $0.89 \mu\text{m}$ come into their own. Broad water bands around $0.94 \mu\text{m}$, $1.15 \mu\text{m}$, $1.5 \mu\text{m}$ and $1.85 \mu\text{m}$ that help to define the Z , J , and H bands are always in evidence, particularly for the 0.2 and 1.0 AU models that don't contain water clouds. For greater distances, the presence of water clouds slightly mutes the variation with wavelength in the planetary spectra. Hence, smoothed water features and methane bands predominate beyond ~ 1.5 AU.

⁷ Note that with a significant eccentricity, this assumption is not valid.

4. AGE DEPENDENCE FROM 100 MYR TO 5 GYR OF THE SPECTRUM OF A $1-M_J$ EGP AT A GIVEN DISTANCE

Figure 6 presents the planet-to-star flux ratios from $0.5 \mu\text{m}$ to $6.0 \mu\text{m}$ for a $1-M_J$ EGP orbiting a G2V star at 4 AU as a function of age. Figure 2 depicts the corresponding T/P profiles, along with the NH_3 and H_2O condensation lines at solar metallicity. The theory of Burrows et al. (1997) is used to obtain an approximate mapping between mass, age, internal T_{eff} , and gravity⁸. The depicted ages are 0.1, 0.3, 1, 3, and 5 Gyr. These planet parameters are chosen merely to represent the systematics with age; different EGP masses and orbital distances will yield quantitatively different spectra. Table 2 shows that for this suite of models the internal flux T_{eff} varies from 290 K to 103 K, the surface gravity varies from 1695 cm s^{-2} to 2325 cm s^{-2} , and the planet radius varies from $1.17 R_J$ to $1.0 R_J$.

As is clear from Fig. 6, younger EGPs with higher inner boundary T_{eff} s (Table 2) have much higher fluxes in the Z , J , H , K , and M bands. However, the older objects, having cooled more, have lower internal luminosities. This results in lower fluxes in those same bands by as much as two orders of magnitude. As Figure 2 shows, the older EGPs have progressively deeper water clouds. What is not obvious from Figure 2 is that these clouds are also thicker. This results in a very slightly increasing reflected optical flux with increasing age that accompanies the reverse trend in the near infrared. Hence, the fluxes in the optical shortward of $\sim 1.0 \mu\text{m}$ are only weak functions of age, while the fluxes in the Z , J , H , K , and M bands at early ages are strong functions of age. At later ages, the formation of water clouds moderates the age dependence of the Z , J , H , and K band fluxes. In fact, there can be slight increases in flux in the Z , J , and H bands with increasing age. However, the M band flux continues to be diagnostic of age, monotonically decreasing by almost two orders of magnitude from 0.1 to 5 Gyr. Hence, the best diagnostics of age are in the near infrared, not the optical.

5. IRRADIATED EGP SPECTRA AS A FUNCTION OF MASS FROM $0.5M_J$ TO $8M_J$ AT A GIVEN AGE AND ORBITAL DISTANCE

Figure 7 portrays planet-to-star flux ratios from $0.4 \mu\text{m}$ to $6.0 \mu\text{m}$ for a 5-Gyr EGP orbiting a G2V star at 4 AU, as a function of EGP mass. The masses represented are 0.5, 1, 2, 4, 6, and $8 M_J$. An inner flux boundary condition T_{eff} from the evolutionary calculations of Burrows et al. (1997) has been employed and is given in Table 3. T_{eff} varies from 82 K to 251 K, the surface gravity varies from 1290 cm s^{-2} to 17800 cm s^{-2} , and the radii vary from $0.95 R_J$ to $1.04 R_J$. Note that these radii peak in the middle of the sequence near $4 M_J$. Due to the 5-Gyr age assumed, all these models have water clouds and the derived modal particle sizes decrease monotonically with increasing mass from $146 \mu\text{m}$ at $0.5 M_J$ to $39 \mu\text{m}$ at $8 M_J$. In general, the larger the EGP mass, the higher in the atmosphere the clouds form, but cloud position is not fully monotonic at the low-mass end of the sequence.

For higher mass, at a given age an EGP's inner T_{eff} and internal luminosity are higher. This results in higher fluxes in the Z , J , H , K , and M bands for higher masses and is similar to the trend seen in §4 with decreasing age. However, larger-mass EGPs also have higher surface gravities, which result in water clouds with lower column depths, and, hence, lower optical

depths, despite the contrary trend of modal particle size (Table 3). The upshot is that higher-mass EGPs have slightly smaller planet/star flux ratios in the optical. This optical component is due to reflection off of cloudy atmospheres with roughly similar compositions. Hence, there is an anti-correlation between flux levels in the visible and near-infrared that might be diagnostic of planet mass for Jupiter-aged EGPs.

6. IRRADIATED BROWN DWARFS

Depicted in Fig. 8 are theoretical spectra of a $30-M_J$ brown dwarf at ages of 1 and 5 Gyr in orbit around a G2V star from $0.4 \mu\text{m}$ to $1.5 \mu\text{m}$. The results are for orbital distances from 5 AU to 40 AU and a distance to the Earth of 10 parsecs and include irradiation effects. As before, the theory of Burrows et al. (1997) is used to determine T_{eff} and gravity for this mass and these ages. In Fig. 8, the prominence of the Na-D ($0.589 \mu\text{m}$) and K I ($0.77 \mu\text{m}$) features at shorter wavelengths is clear and is canonical for brown dwarfs (Burrows, Marley, and Sharp 2000).

Unlike for the lower mass EGPs discussed in §3, §4, and §5, the internal luminosity of such a relatively massive SMO dominates its energy budget. As a consequence, the brown dwarf's spectrum longward of $0.9 \mu\text{m}$ is unaffected by irradiation. However, the reflected component in the optical, particularly for the older brown dwarf with lower internal heat content and luminosity, is a function of distance. As Fig. 8 demonstrates, the optical flux from a cool brown dwarf can be elevated shortward of $0.7 \mu\text{m}$ by as much as an order of magnitude in the V band. In particular, the shape of the Na-D feature can be significantly altered. Since there are no clouds in the atmospheres of these brown dwarf models, Rayleigh scattering off of H_2 , He, and H_2O accounts for this reflection. Our prediction is that the optical spectra of brown dwarfs that are close companions to K, G, or F stars will be modified by irradiation. Note that the T dwarf Gliese 229B is at a projected distance of ~ 40 AU, but that its primary is an M4V star. Such a star is too dim to so radically alter a brown dwarf's optical flux. For an L dwarf companion, the presence of silicate clouds in its atmosphere will reflect a primary's light in the blue and UV. Someday, such a reflected component might be detectable.

7. PREDICTED PHASE-AVERAGED SPECTRA FOR KNOWN EGPS AT WIDE ANGULAR SEPARATIONS

Table 4 lists many of the known EGPs that, due to a propitious combination of semi-major axis and distance from the Earth, are at wide angular separations from their parent stars⁹. Ordered by decreasing separation (defined as the ratio of semi-major axis to distance), Table 4 also lists the stellar type of the primary, semi-major axis, Hipparcos distance, orbital period, $m_p \sin(i)$, and orbital eccentricity. This family of known EGP comprises some of the prime candidates for direct detection of planetary light using interferometric, adaptive-optics, or coronagraphic techniques (§1). Note that the separations quoted in Table 4 don't take into account the projection of the orbit or variations due to non-zero eccentricities (which can be large). In particular, variations due to the significant excursions in planet-star distance that attend large eccentricities can result in large changes in irradiation regimes. In turn, this can result in large variations in planet spectrum. Interestingly, it is possible

⁸ We note that the star evolves as well, but for clarity we have neglected this effect.

⁹ For comparison, some of the closest EGPs are also shown at the bottom of Table 4.

for an EGP atmosphere to cycle between states with and without clouds, with the concomitant large changes in flux ratios and spectral signatures with orbital phase (Sudarsky, Burrows, and Hubeny 2004). Figure 3 gives some idea of the range of spectral variation possible for highly-eccentric EGPs.

Figures 3, 6, and 7 provide a broad-brush view of generic EGP spectra for a range of orbital distances, ages, and masses. With Figs. 9, 10, and 11, we provide phase-averaged predictions/calculations for a specific subset of the known EGPs listed in Table 4. This subset includes HD 39091b, γ Cephei b, HD 70642b, v And d, Gliese 777A b, HD 216437b, HD 147513b, 55 Cancri d, 47 UMa b, 47 UMa c, 14 Her b, and ϵ Eri b. Table 5 itemizes these EGPs, along with their derived T_{eff} s and surface gravities. In addition, Table 5 lists the theoretical modal particle sizes of the water droplets that form in their atmospheres. For definiteness, the planetary masses are set equal to the measured $m_p \sin(i)$ and, as before, the evolutionary theory of Burrows et al. (1997) is used to estimate the corresponding surface gravities and inner boundary T_{eff} s. As described in SBH and §2, a stellar spectrum from Kurucz (1994) for the primary stellar type given for each EGP in Table 5 is used for the outer irradiation boundary condition in the self-consistent atmosphere/spectrum calculation. As a comparison of Figs. 3, 4, and 5 with Figs. 9, 10, and 11 demonstrates, the major dependence of the planet-to-star flux ratio is with orbital distance. Note that for all of the EGPs listed in Table 5, the assumption that the planet-star distance is fixed at the measured semi-major axis does not result in the formation of ammonia clouds. However, such clouds should form near apastron for the known EGPs with large semi-major axes and high eccentricities, such as ϵ Eri b and 55 Cnc d. The appearance and disappearance of such clouds with orbital phase would be exciting signatures to detect.

8. SUMMARY AND CONCLUSIONS

In this paper, we have calculated theoretical phase-averaged planet/star flux ratios in the optical, near-infrared, and mid-infrared for wide-separation irradiated EGPs as a function of orbital distance, mass, and age. We have also predicted the corresponding quantities for 12 specific known EGPs, given their corresponding primary spectra, average orbital distances, approximate masses, and approximate ages. Hence, we have explored various physical diagnostics that can inform the direct EGP detection programs now being planned or proposed. In the optical, the flux ratios for distances from 0.2 AU to 15 AU and masses from $0.5 M_J$ to $8 M_J$ can vary from slightly above 10^{-8} to $\sim 10^{-10}$. In the near infrared around 2-4 μm , the flux ratio ranges more widely, spanning values from 10^{-4} to as low as 10^{-16} . At $\sim 5 \mu\text{m}$, the planet/star flux ratio ranges approximately four orders of magnitude and can be as high as 10^{-4} . The M band should be a useful region to explore and M -band fluxes are sensitive to the presence of clouds. For all models, the mid-infrared from 10 μm to 30 μm is always encouragingly high. In fact, for closer separations (0.05 AU-0.1 AU), not the subject of this paper, the flux ratio at $\sim 20 \mu\text{m}$ can be $\sim 10^{-3}$.

Depending upon orbital distance, age, and mass, spectral features due to methane, water, and the alkali metals are prominent. Furthermore, there is a slight anti-correlation in the effects of clouds in the optical and infrared, with the optical fluxes

increasing and the infrared fluxes decreasing with increasing cloud depth. For young and massive irradiated EGPs, there are prominent peaks in the Z , J , H , K , and M bands. Though the optical flux is not a very sensitive function of age, there is a useful age dependence of the fluxes in these bands. Furthermore, there is an anti-correlation with increasing mass at a given age and orbital distance between the change in flux in the optical and in the near-IR bands, with the optical fluxes decreasing and the Z , J , H , K , and M band fluxes increasing with increasing mass.

The spectra of more massive SMOs (brown dwarfs) longward of $\sim 0.9 \mu\text{m}$ are not significantly affected by stellar irradiation. Their internal heat content and interior fluxes are too large. However, brown dwarf fluxes from 0.4 μm to 0.65 μm , can be enhanced by Rayleigh reflection by as much as a factor of 10. This is particularly true of old or low-mass brown dwarfs and is a predictable function of distance. Moreover, irradiation can alter the profile shape of the Na-D feature significantly.

We are not able to calculate EGP spectra for all possible combinations of mass, age, composition, orbital distance, eccentricity, orbital phase, Keplerian element, and primary spectral type. This fact is what motivates the more modest synoptic view we have provided in this paper. However, in the process of developing the tools for this study, we have established the capability to calculate EGP spectra for any combination of these parameters. In particular, Sudarsky, Burrows, and Hubeny (2004) address the orbital phase and eccentricity dependences of irradiated EGPs spectra.

The remote sensing of the atmospheres of EGPs will be challenging, but the detection and characterization of the direct light from a planet outside our solar system will be an important milestone in both astronomy and planetary science. One instrument proposed to meet this challenge is the space-based coronagraphic imager *Eclipse* (Trauger et al. 2000,2001). The *Eclipse* instrument team is predicting a contrast capability of $\sim 10^{-9}$ for an inner working angle of 0.3'' or 0.46'' in the V/R or Z bands, respectively. As Figs. 3 through 7 indicate, with such a capability irradiated EGPs could be detected and analyzed. Many could even be discovered. However, whether such sensitivity is achievable remains to be demonstrated. Be that as it may, further advancement in our understanding of extrasolar planets is contingent upon technical advances that would enable the direct measurement of the dynamically dominant and brighter components of extrasolar planetary systems, the EGPs.

The authors wish to acknowledge Bill Hubbard, Jonathan Lunine, Jim Liebert, John Trauger, Jonathan Fortney, Aigen Li, Christopher Sharp, Drew Milsom, Maxim Volobuyev, and Curtis Cooper for fruitful conversations or technical aid and help during the course of this work, as well as NASA for its financial support via grants NAG5-10760 and NAG5-10629. Furthermore, we acknowledge support through the Cooperative Agreement #NNA04CC07A between the University of Arizona/NOAO LAPLACE node and NASA's Astrobiology Institute. Finally, the first author would also like to thank the Kavli Institute for Theoretical Physics where some of this work was performed.

REFERENCES

- Akeson, R. L. & Swain, M. R. 2000, in *From Giant Planets to Cool Stars*, ed. C. A. Griffith & M. S. Marley, ASP Conference Series, 212, 300
- Akeson, R. L., Swain, M. R., & Colavita, M. M. 2000, in *Interferometry in Optical Astronomy*, ed. P. J. Lena, Proc. SPIE 4006, 321
- Anders, E. & Grevesse, N. 1989, *Geochim. Cosmochim. Acta*, 53, 197
- Antonello, E. & Ruiz, S. M. 2002, *The Corot Mission*, <http://www.astrsp-mrs.fr/projects/corot/corotmission.ps>
- Baraffe, I., Chabrier, G., Allard, F., and Hauschildt, P.H. 2003, *Astron. Astrophys.*, 402, 701
- Bennett, G.F. et al. 2002, *ApJ*, 581, L115
- Brown, T. M., Charbonneau, D., Gilliland, R.L., Noyes, R.W., and Burrows, A. 2001, *ApJ*, 552, 699
- Burrows, A., Saumon, D., Guillot, T., Hubbard, W.B., & Lunine, J.I. 1995, *Nature*, 373, 191
- Burrows, A. & Lunine, J.I. 1995, *Nature*, 378, 333
- Burrows, A., Marley, M., Hubbard, W. B., Lunine, J. I., Guillot, T., Saumon, D., Freedman, R., Sudarsky, D., & Sharp, C. 1997, *ApJ*, 491, 856
- Burrows, A. & Sharp, C. M. 1999, *ApJ*, 512, 843
- Burrows, A., Marley, M.S., & Sharp, C.M. 2000, *ApJ*, 531, 438
- Burrows, A., Hubbard, W.B., Lunine, J.I., & Liebert, J. 2001, *Rev. Mod. Phys.*, 73, 719
- Burrows, A., Sudarsky, D., & Hubbard, W.B. 2003, *ApJ*, 594, 545
- Burrows, A., Sudarsky, D., & Lunine, J.I. 2003, *ApJ*, 596, 587
- Butler, R. P., Marcy, G. W., Williams, E., Hauser, H. & Shirts, P. 1997, *ApJ*, 474, L115
- Butler, R. P., Marcy, G. W., Fischer, D. A., et al. 1999, *ApJ*, 526, 916
- Castor, J. I., Dykema, P. G., & Klein, R. I. 1992, *ApJ*, 387, 561
- Charbonneau, D., Brown, T. M., Latham, D. W., & Mayor, M. 2000, *Astrophys. J. Letters*, 529, L45
- Charbonneau, D., Brown, T. M., Noyes, R. W., Gilliland, R. L., and Burrows, A. 2001, *ApJ*, 552, 891
- Charbonneau, D., Brown, T. M., Noyes, R. W., & Gilliland, R. L. 2002, *ApJ*, 568, 377
- Christensen-Dalsgaard, J. 2000, <http://bigcat.obs.aau.dk/hans/mons/>
- Cooper, C. S., Sudarsky, D., Milsom, J. A., Lunine, J. I., & Burrows, A. 2003, *ApJ*, 586, 1320
- Deirmendjian, D. 1964, *Applied Optics*, 3, 187
- Deirmendjian, D. 1969, *Electromagnetic Scattering on Spherical Polydispersions*, (New York: Elsevier)
- Fortney, J.J., Sudarsky, D., Hubeny, I., Cooper, C.S., Hubbard, W.B., Burrows, A., & Lunine, J.I. 2003, *ApJ*, 589, 615
- Goukenleuque, C., Bezar, B., Joguuet, B., Lellouch, E., & Freedman, R. 2000, *Icarus*, 143, 308
- Henry, G., Marcy, G. W., Butler, R. P., & Vogt, S. S. 2000, *ApJ*, 529, L41
- Hinz, P. M. 2001, PhD Thesis, The University of Arizona
- Hubeny, I. 1988, *Computer Physics Comm.*, 52, 103
- Hubeny, I. & Lanz, T. 1995, *ApJ*, 439, 875
- Koch, D., Borucki, W., Webster, L., Dunham, E., Jenkins, J., Marrion, J., & Reitsema, H. 1998, SPIE Conference 3356: *Space Telescopes and Instruments V*, 599
- Konacki, M., Torres, G., Jha, S., and Sasselov, D. 2003, *Nature*, 421, 507
- Kurucz, R. 1994, *Kurucz CD-ROM No. 19*, (Cambridge: Smithsonian Astrophysical Observatory)
- Levine, B.M. et al. 2003, SPIE, 4852, 221
- Lodders, K. 1999, *ApJ*, 519, 793
- Lodders, K. & Fegley, B. 2002, *Icarus*, 155, 393
- Marcy, G. W. and R.P. Butler 1996, *ApJ*, 464, L147
- Marcy, G. W., Butler, R. P., Vogt, S. S., Fischer, D., & Lissauer J. J. 1998, *ApJ*, 505, L147
- Marcy, G. W., R.P. Butler, S.S. Vogt, D. Fischer, and M.C. Liu 1999, *ApJ*, 520, 239
- Marcy, G.W., W. Cochran, and M. Mayor, 2000, in *Protostars and Planets IV*, ed. V. Mannings, A.P. Boss, and S.S. Russell (Tucson: The University of Arizona Press), p. 1285-1311
- Marley, M. S., Gelino, C., Stephens, D., Lunine J. I., & Freedman, R. 1999, *ApJ*, 513, L879
- Matthews, J. M., Kuschnig, R., Walker, G. A. H. et al. 2001, in *The Impact of Large-Scale Surveys on Pulsating Star Research*, ed. L. Szabados & D. Kurtz, p. 74
- Mayor, M. & Queloz, D. 1995, *Nature*, 378, 355
- Paresce, F. 2001, *Scientific Objectives of the VLTI Interferometer*
- Queloz, D., M. Mayor, L. Weber, A. Blécha, M. Burnet, B. Confino, D. Naef, F. Pepe, N. Santos, and S. Udry 2000, *Astron. Astrophys.*, 354, 99
- Santos, N.C., M. Mayor, D. Naef, F. Pepe, D. Queloz, S. Udry, M. Burnet, and Y. Revaz 2000, *Astron. Astrophys.*, 356, 599
- Seager, S. & Sasselov, D. D. 1998, *ApJ*, 502, 157
- Seager, S., Whitney, B. A., & Sasselov, D. D. 2000, *ApJ*, 540, 504
- Seager, S. & Sasselov, D. D. 2000, *ApJ*, 537, 916
- Sudarsky, D., Burrows, A., & Pinto, P. 2000, *ApJ*, 538, 885
- Sudarsky, D., Burrows, A., & Hubeny, I. 2003, *ApJ*, 588, 1121
- Sudarsky, D., Burrows, A., & Hubeny, I. 2004, in preparation
- Torres, G., Konacki, M., Sasselov, D., and Jha, S. 2003, *astro-ph/0310114*
- Trauger, J., Backman, D., Brown, R. A. et al. 2000, AAS Meeting 197, 49.07
- Trauger, J., Hull, A. B., & Redding, D. A. 2001, AAS Meeting 199, 86.04
- Unwin, S. C. & Shao, M. 2000, in *Interferometry in Optical Astronomy*, ed. P. J. Lena & A. Quirrenbach, 754
- van Belle, G. & Vasisht, G. 1998, *The Keck Interferometer Science Requirements Document, Revision 2.2*, Jet Propulsion Laboratory
- Vidal-Madjar, A., des Etangs, A., Desert, J.-M., Ballester, G.E., Ferlet, R., Hebrard, G., Mayor, M. 2003, *Nature*, 422, 143
- Werner, M.W. and Fanson, J.L. 1995, *Proc. SPIE*, 2475, p. 418-427

TABLE 1
MODEL DATA FOR DISTANCE SEQUENCE

a (AU)	condensate(s)	r_0 (μm)
0.2	none	-
0.5	none	-
1	none	-
2	H ₂ O	107
4	H ₂ O	109
6	NH ₃ , H ₂ O	56, 110
8	NH ₃ , H ₂ O	56, 111
10	NH ₃ , H ₂ O	57, 111
15	NH ₃ , H ₂ O	62, 111

TABLE 2
MODEL DATA FOR AGE SEQUENCE

Age (Gyr)	T_{eff} (K)	$\log_{10} g$ (cm s $^{-2}$)	R/R_J	r_0 (μm)
0.1	290	3.23	1.17	123
0.3	219	3.27	1.11	119
1	159	3.31	1.06	123
3	118	3.35	1.02	111
5	103	3.37	1.00	109

TABLE 3
MODEL DATA FOR MASS SEQUENCE

M/M_J	T_{eff} (K)	$\log_{10} g$ (cm s $^{-2}$)	R/R_J	r_0 (μm)
0.5	82	3.11	0.95	146
1	103	3.37	1.00	109
2	134	3.64	1.03	80
4	177	3.93	1.04	57
6	216	4.12	1.03	46
8	251	4.25	1.02	39

TABLE 4
INTERESTING EGPs LISTED BY ANGULAR SEPARATION

EGP	separation ($''$)	star	a (AU)	d (pc)	P	$M \sin i$ (M_J)	e
ϵ Eri b	1.0	K2V	3.3	3.2	6.85 yrs.	0.86	0.61
55 Cnc d	0.44	G8V	5.9	13.4	14.7	4.05	0.16
47 UMa c	0.28	G0V	3.73	13.3	7.10	0.76	0.1
GI 777A b	0.23	G6V	3.65	15.9	7.15	1.15	~ 0
ν And d	0.19	F8V	2.50	13.5	3.47	4.61	0.41
HD 39091b	0.16	G1IV	3.34	20.6	5.70	10.3	0.62
47 UMa b	0.16	G0V	2.09	13.3	2.98	2.54	0.06
γ Cephei b	0.15	K2V	1.8	11.8	2.5	1.25	~ 0
HD 160691c	0.15	G3IV-V	2.3	15.3	3.56	~ 1	~ 0.8
14 Her b	0.15	K0V	2.5	17	4.51	3.3	0.33
HD 33636b	0.12	G0V	3.56	28.7	4.43	7.71	0.41
HD 10647b	0.12	F9V	2.10	17.3	2.89	1.17	0.32
HD 70642b	0.11	G5IV-V	3.3	29	4.79	2.0	0.10
HD 216437b	0.10	G4V	2.7	26.5	3.54	2.1	0.34
HD 147513b	0.098	G3V	1.26	12.9	1.48	1.0	0.52
HD 160691b	0.097	G3IV-V	1.48	15.3	1.74	1.7	0.31
HD 168443c	0.087	G5V	2.87	33	4.76	17.1	0.23
HD 50554b	0.077	F8V	2.38	31.03	3.50	4.9	0.42
HD 106252b	0.070	G0V	2.61	37.44	4.11	6.81	0.54
HD 10697b	0.067	G5IV	2.0	30	2.99	6.59	0.12
ν And c	0.061	F8V	0.83	13.5	241 days	2.11	0.18
GJ 876b	0.045	M4V	0.21	4.72	61.0	1.89	0.1
GJ 876c	0.028	M4V	0.13	4.72	30.1	0.56	0.27
HD 114762b	0.013	F9V	0.35	28	84.0	11.0	0.34
55 Cnc b	8.2×10^{-3}	G8V	0.12	13.4	14.7	0.84	0.02
ν And b	4.4×10^{-3}	F8V	0.059	13.5	4.62	0.71	0.034
51 Peg b	3.4×10^{-3}	G2V	0.05	14.7	4.23	0.44	0.01
τ Boo b	3.3×10^{-3}	F7V	0.05	15	3.31	4.09	~ 0
HD 209458b	9.6×10^{-4}	G0V	0.045	47	3.52	0.69	~ 0
HD 83443b	8.7×10^{-4}	K0V	0.038	43.5	2.99	0.35	0.08

TABLE 5
MODEL DATA FOR SPECIFIC EGPs

EGP	star	a (AU)	d (pc)	$M \sin i$	T_{eff} (K)	$\log_{10} g$ (cgs)	r_0 (μm)
ϵ Eri b	K2V	3.3	3.2	0.86	170	3.48	5 ¹
55 Cnc d	G8V	5.9	13.4	4.05	200	4.30	5 ¹
47 UMa c	G0V	3.73	13.3	0.76	95	3.48	96
G1 777A b	G6V	3.65	15.9	1.15	100	3.48	97
ν And d	F8V	2.50	13.5	4.61	250	4.30	5 ¹
HD 39091b	G1IV	3.34	20.6	10.3	300	4.48	-
47 UMa b	G0V	2.09	13.3	2.54	150	3.78	67
γ Cephei b	K2V	1.8	11.8	1.25	150	3.60	83
14 Her b	K0V	2.5	17	3.3	150	3.90	59
HD 70642b	G5V	3.3	29	2.0	130	3.64	80
HD 216437b	G4V	2.7	26.5	2.1	150	3.70	72
HD 147513b	G3V	1.26	12.9	1.0	100	3.37	96

References. — 1) From Sudarsky, Burrows, & Hubeny (2003), where a modal particle size of 5 μm was assumed.

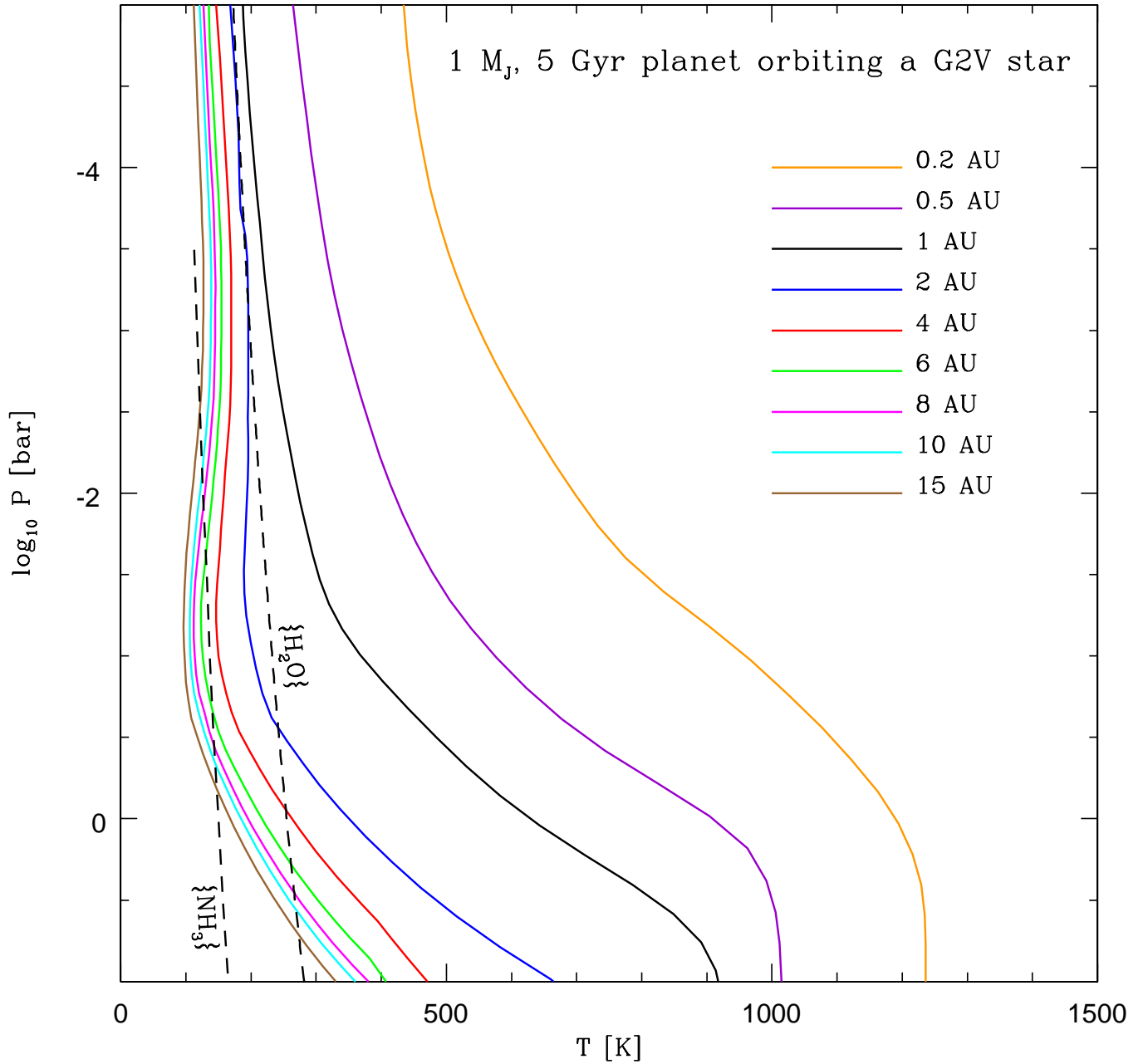


FIG. 1.— Profiles of atmospheric temperature (in Kelvin) versus the logarithm base ten of the pressure (in bars) for a family of irradiated $1-M_J$ EGPs around a G2V star as a function of orbital distance. Note that the pressure is decreasing along the ordinate, which thereby resembles altitude. The orbits are assumed to be circular, the planets are assumed to have a radius of $1 R_J$, the effective temperature of the inner boundary flux is set equal to 100 K, and the orbital separations vary from 0.2 AU to 15 AU. The intercepts with the dashed lines identified with either $\{NH_3\}$ or $\{H_2O\}$ denote the positions where the corresponding clouds form. See text for a discussion.

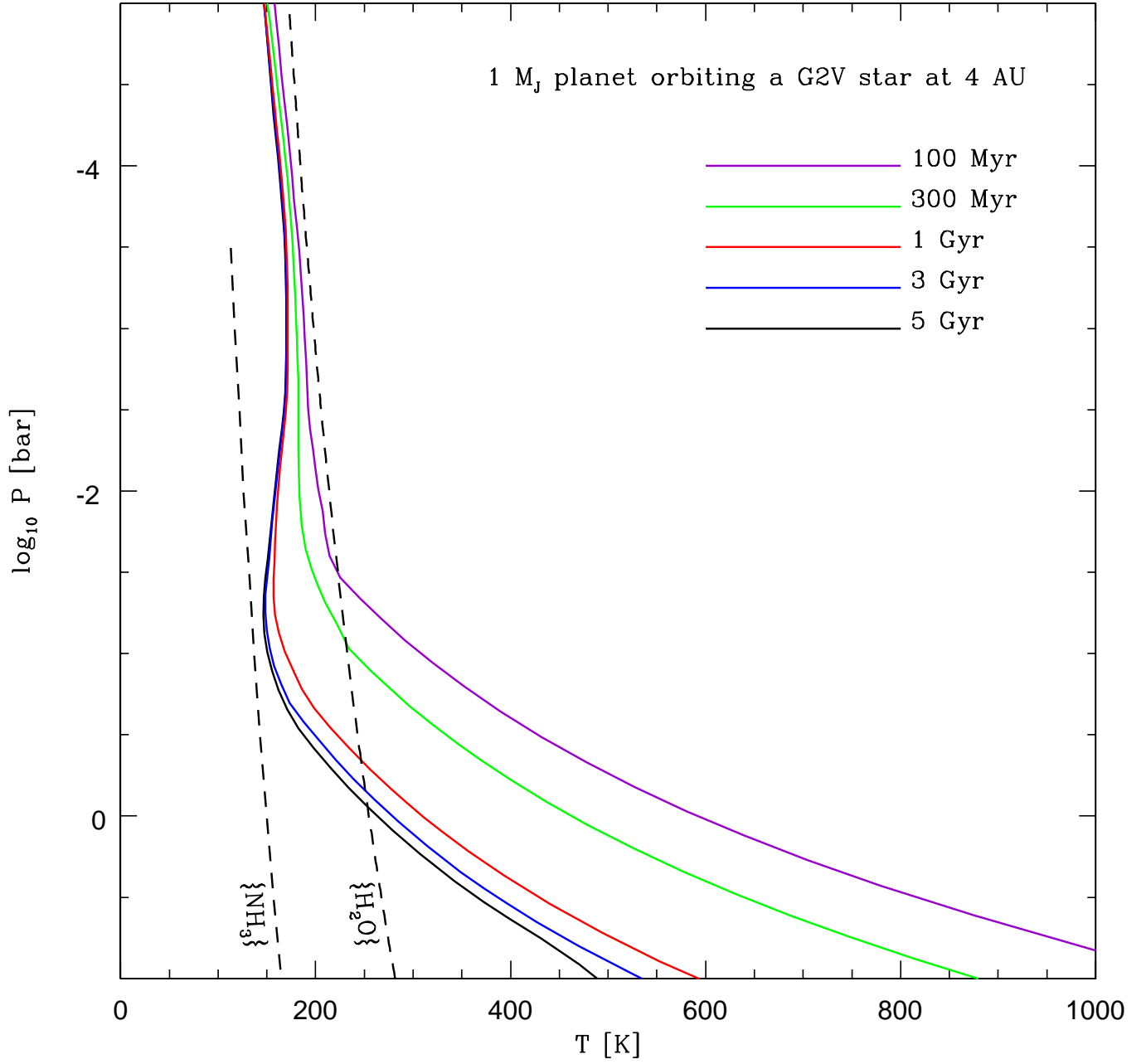


FIG. 2.— Similar to Fig. 1, this figure depicts atmospheric profiles of temperature (in Kelvin) versus the logarithm base ten of the pressure (in bars) for a family of irradiated $1-M_J$ EGPs around a G2V star, but as a function of age at a given orbital distance of 4.0 AU. The ages vary from 0.1 to 5.0 Gyr. Note that the pressure is decreasing along the ordinate, which thereby resembles altitude. The cloud condensation curves for both NH_3 (moot for this sequence) and H_2O are given as the dashed lines and the spectral/atmospheric models include the effects of the water clouds in a consistent way. See text in §3 and §4 for relevant details and discussion.

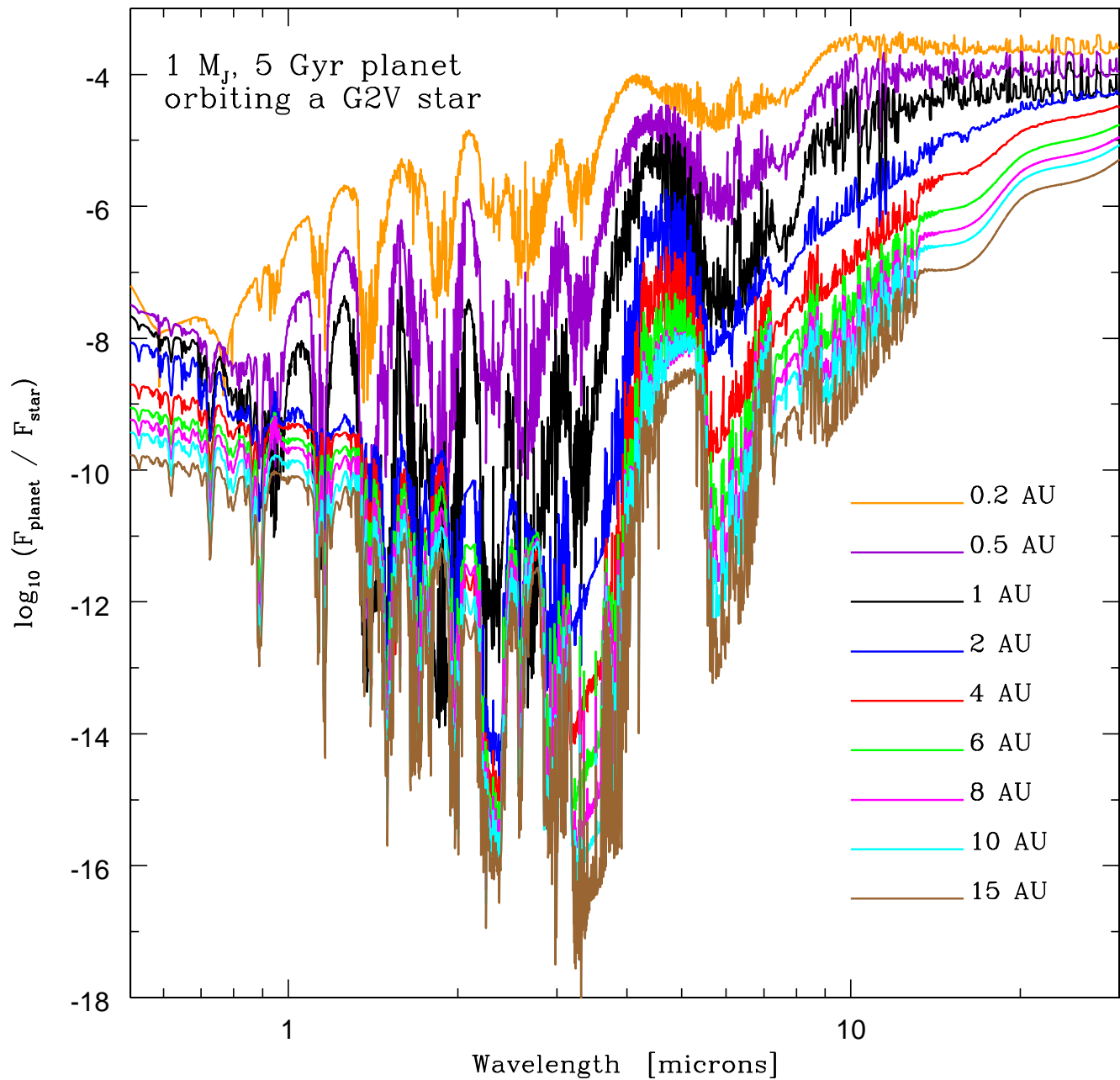


FIG. 3.— Planet to star flux ratios versus wavelength (in microns) from $0.5 \mu\text{m}$ to $30 \mu\text{m}$ for a $1-M_J$ EGP with an age of 5 Gyr orbiting a G2V main sequence star similar to the Sun. This figure portrays ratio spectra as a function of orbital distance from 0.2 AU to 15 AU. Zero eccentricity is assumed and the planet spectra have been phase-averaged as described in Sudarsky, Burrows, and Hubeny (2003). The associated T/P profiles are given in Fig. 1 and Table 1 lists the modal radii for the particles in the water and ammonia clouds. Note that the planet/star flux ratio is most favorable in the mid-infrared. See text for further discussion.

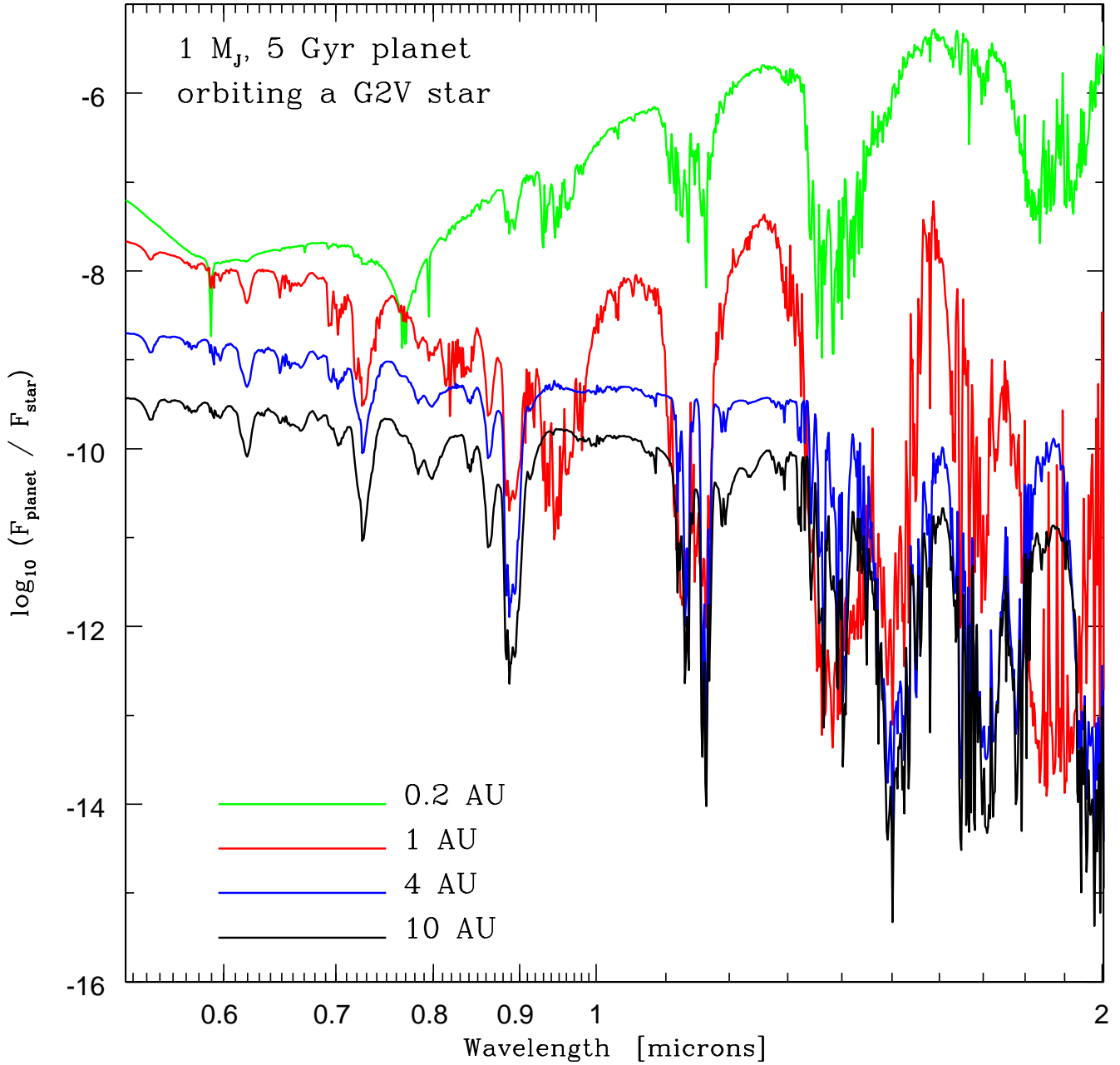


FIG. 4.— The same as Fig. 3, but highlighting the shorter wavelengths and for a subset of distances (0.2, 1, 4, 10 AU). This figure provides a clearer picture of the features shortward of $2.0 \mu\text{m}$ for each of the represented models. For the 0.2 AU model, the temperatures of the atmosphere are high enough for the Na-D doublet around $0.589 \mu\text{m}$ and the K I doublet near $0.77 \mu\text{m}$ to be visible. These features are even more prominent for closer-in EGPs (Sudarsky, Burrows, and Hubeny 2003). At greater orbital distances, the atmospheric temperatures are too low for the alkali metals to appear, but the methane features near $0.62 \mu\text{m}$, $0.74 \mu\text{m}$, $0.81 \mu\text{m}$, and $0.89 \mu\text{m}$ come into their own. Water bands around $0.94 \mu\text{m}$, $1.15 \mu\text{m}$, $1.5 \mu\text{m}$ and $1.85 \mu\text{m}$ that help to define the *Z*, *J*, and *H* bands are always of importance. For greater distances, the presence of water clouds can smooth the variations in the planetary spectra that would otherwise be large due to the strong absorption features of gaseous water vapor. See text for discussion.

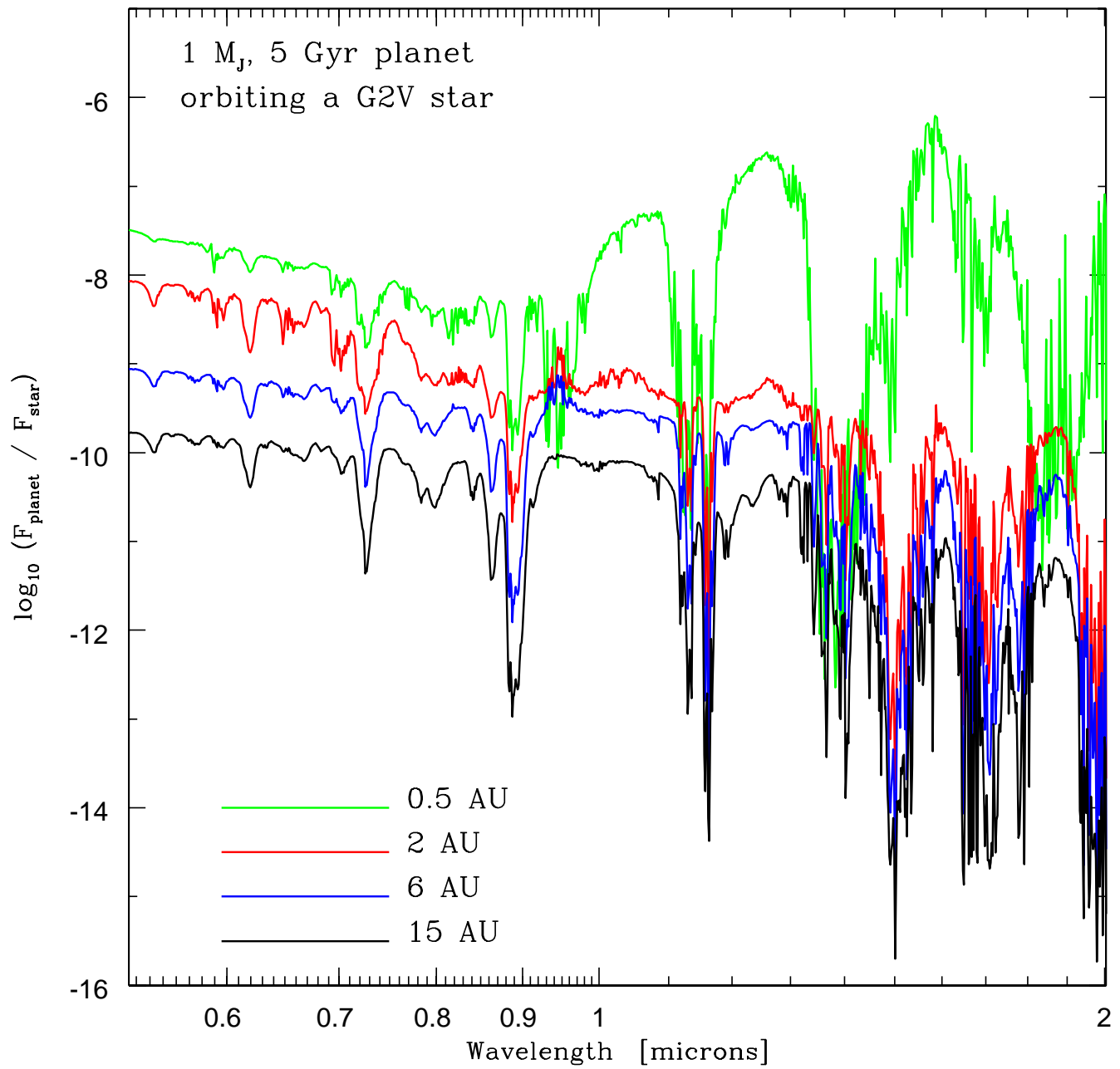


FIG. 5.— The same as Fig. 3, but, as in Fig. 4, highlighting the shorter wavelengths. A different subset of distances (0.5, 2, 6, 15 AU) is shown. See the text and the figure caption for Fig. 4 for details. Figures 4 and 5 allow one to distinguish more easily than is possible in the panoramic Fig. 3 one model from another.

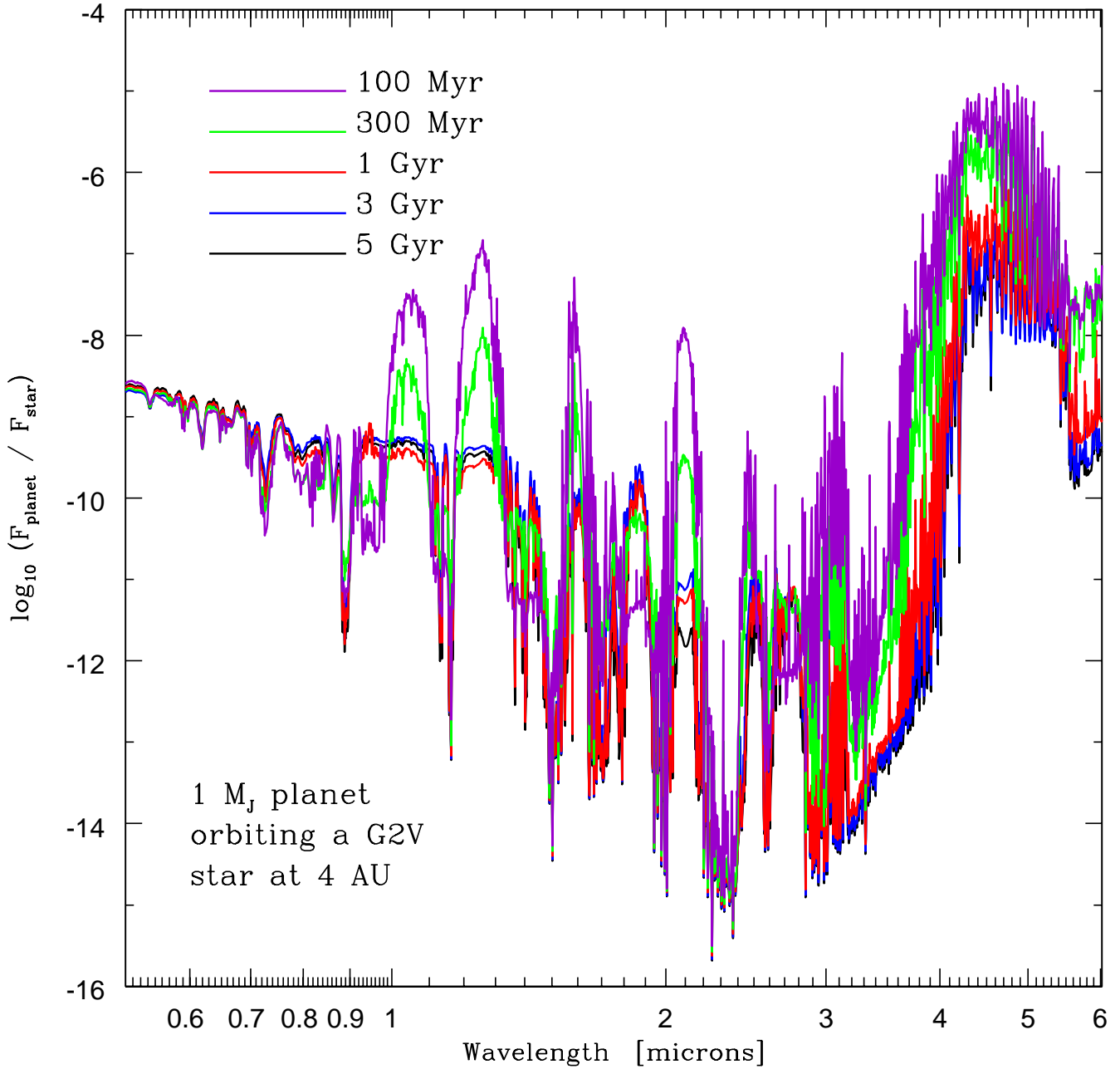


FIG. 6.— The planet-to-star flux ratio from $0.5 \mu\text{m}$ to $6.0 \mu\text{m}$ for a $1-M_J$ EGP orbiting a G2V star at 4 AU as a function of age. The ages are 0.1, 0.3, 1, 3, and 5 Gyr. An inner flux boundary condition T_{eff} from the evolutionary calculations of Burrows et al. (1997) has been employed. The effect of clouds is handled in the radiative transfer calculation in a completely consistent fashion. See Table 2, Figure 2, and text for details and discussion.

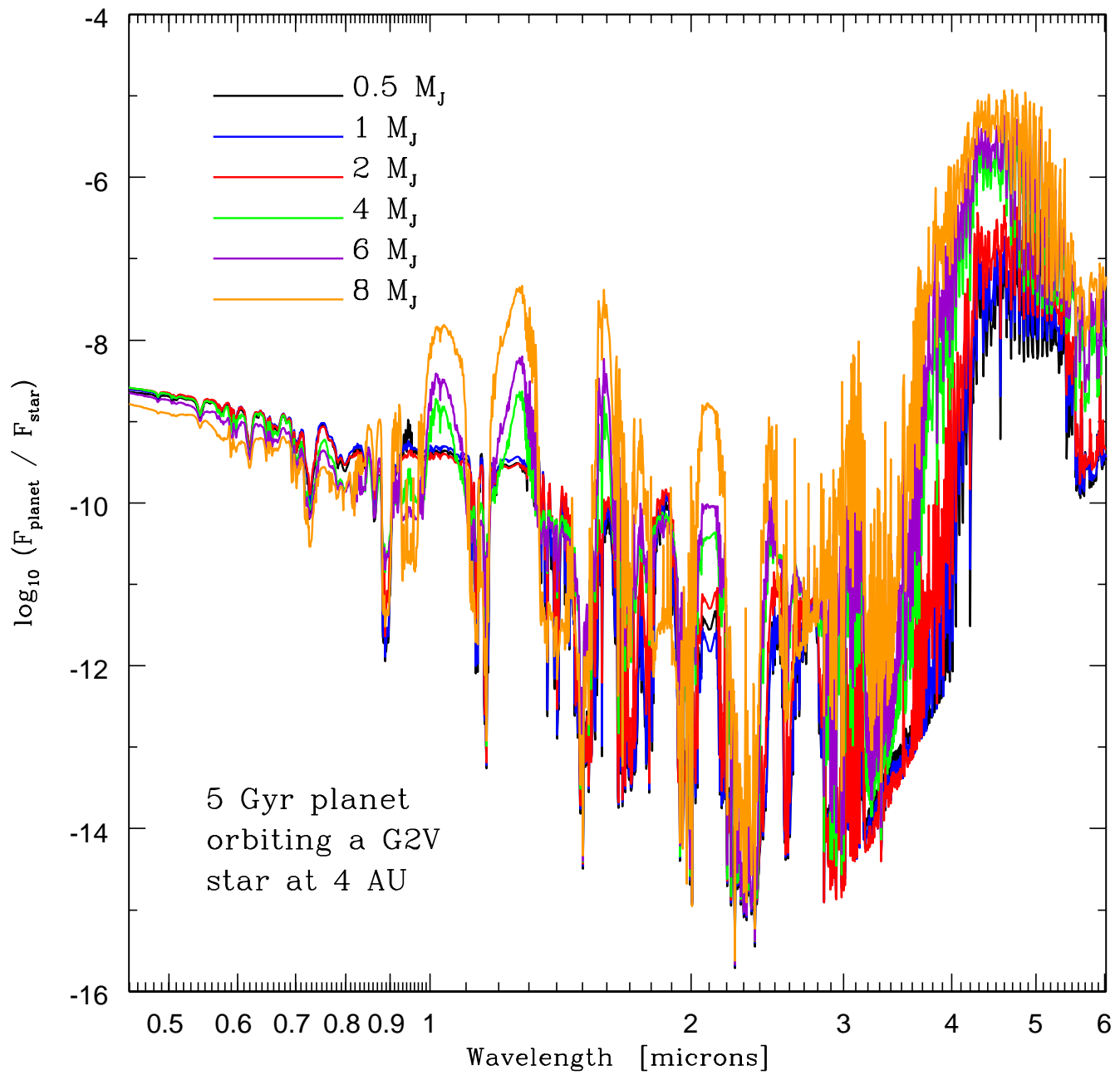


FIG. 7.— Similar to Fig. 6, but the planet-to-star flux ratio from $0.4 \mu\text{m}$ to $6.0 \mu\text{m}$ for a 5-Gyr EGP orbiting a G2V star at 4 AU, as a function of EGP mass. The masses represented are 0.5 , 1 , 2 , 4 , 6 , and $8 M_J$. See Table 3 and text for a discussion.

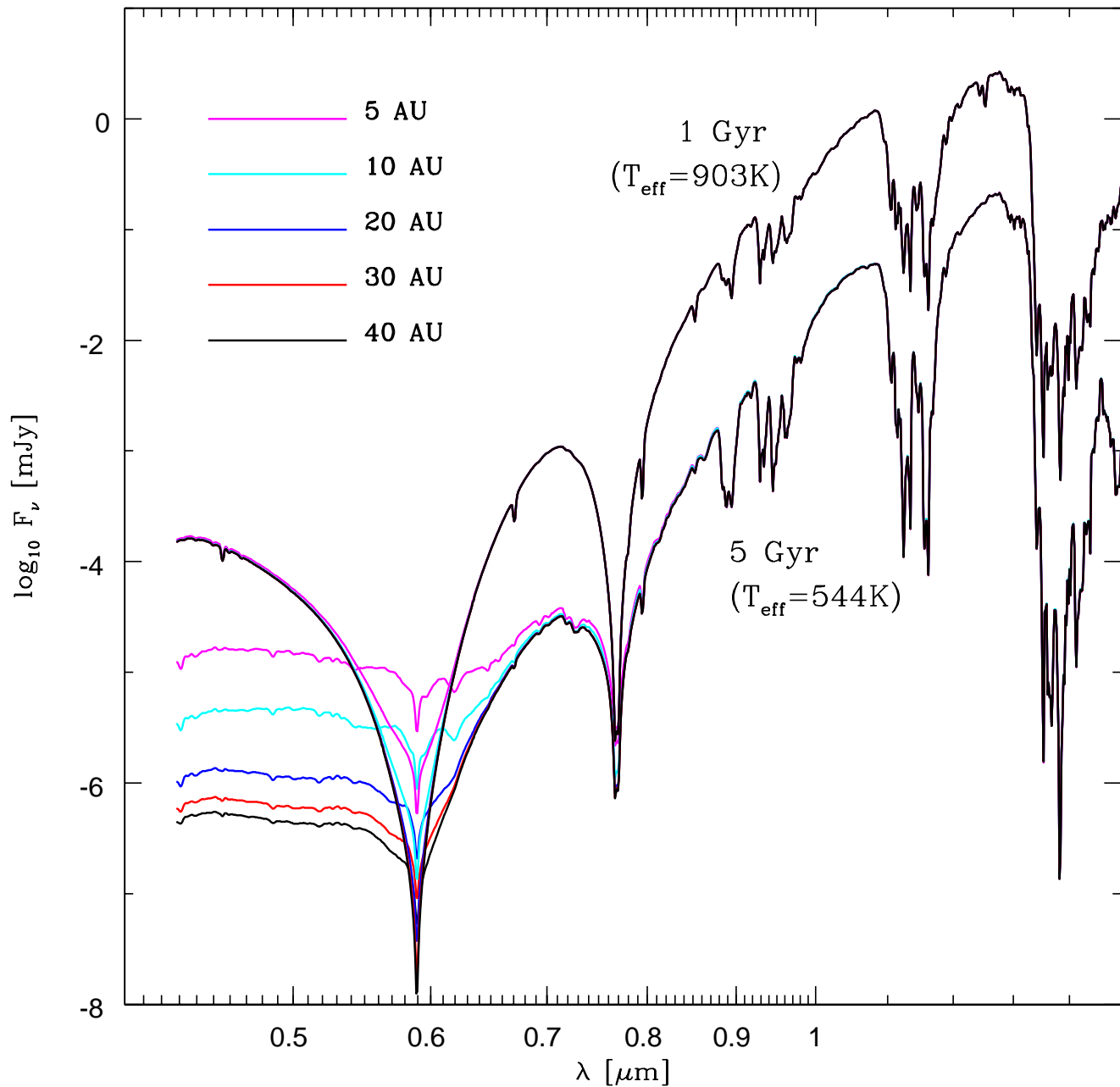


FIG. 8.— Depicted are theoretical spectra of a $30-M_J$ brown dwarf at ages of 1 and 5 Gyr in orbit around a G2V star that is irradiating it. The logarithm base ten of the flux in milliJanskys at 10 parsecs versus wavelength in microns from $0.4 \mu\text{m}$ to $1.5 \mu\text{m}$ is given. The theory of Burrows et al. (1997) was used to determine T_{eff} and gravity for these ages and mass. The results are shown for different orbital distances from 5 to 40 AU. See text for a discussion.

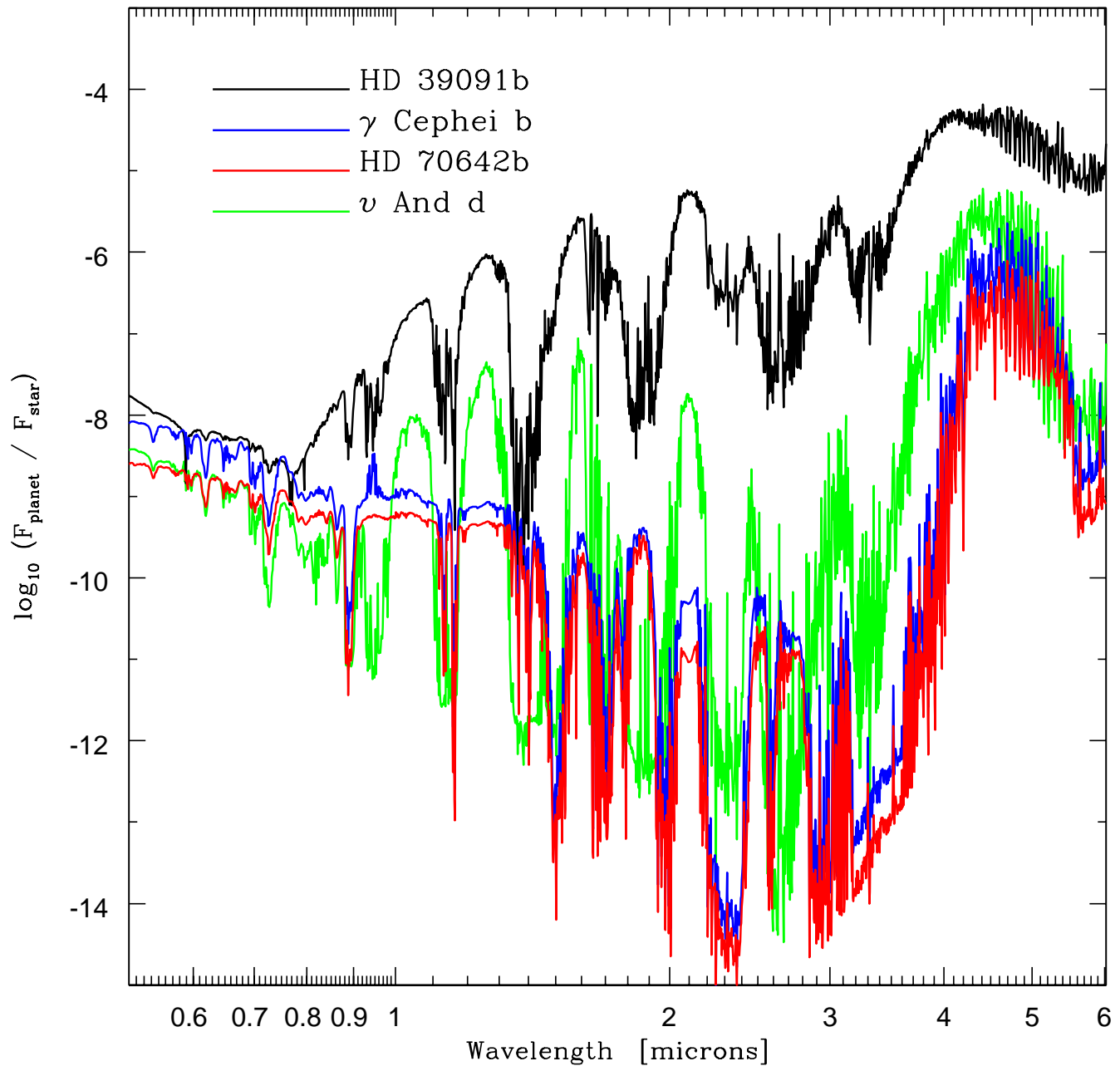


FIG. 9.— Similar to Figs. 6 and 7, but for four specific known EGPs listed in Table 5. These are HD 39091b, γ Cephei b, HD 70642b, and v And d. The wavelengths range from $0.5 \mu\text{m}$ to $6.0 \mu\text{m}$. The planet fluxes are phase-averaged and the effect of the known eccentricities is ignored. The orbital distances are assumed to be equal to the measured semi-major axes and the planets' masses are set equal to the measured values of $m_p \sin(i)$. For all of these objects water clouds are formed and the modal particle sizes are given in Table 5. Table 5 also shows the values of the gravity and the T_{eff} that describes the inner flux, both derived using the theory of Burrows et al. (1997). Compare this figure with Figs. 3, 6, and 7 and see text for details.

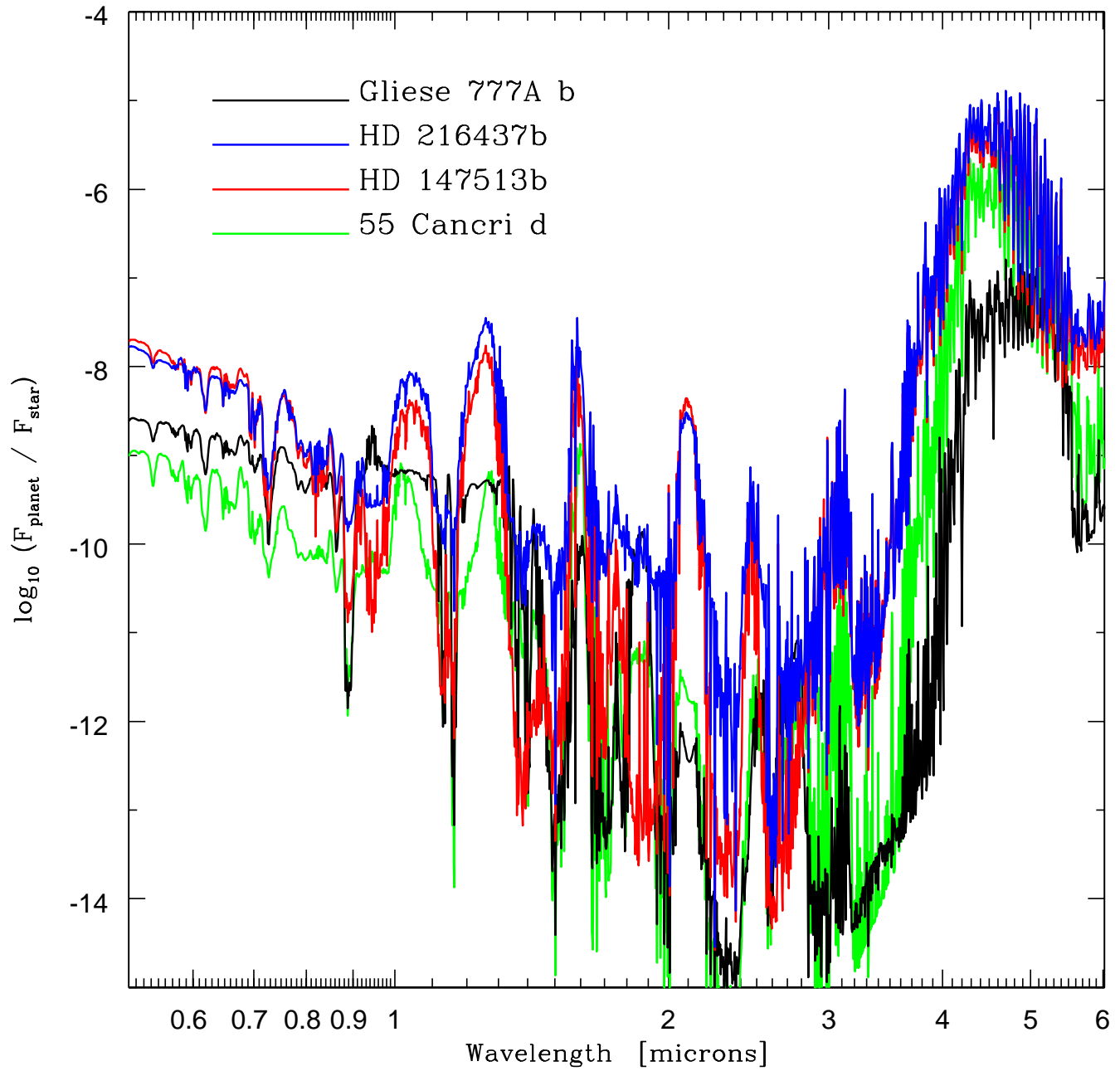


FIG. 10.— Same as Fig. 9, but for Gliese 777A b, HD 216437b, HD 147513b, and 55 Cancri d. Refer to Fig. 9, Table 5, and the text for further details and discussion.

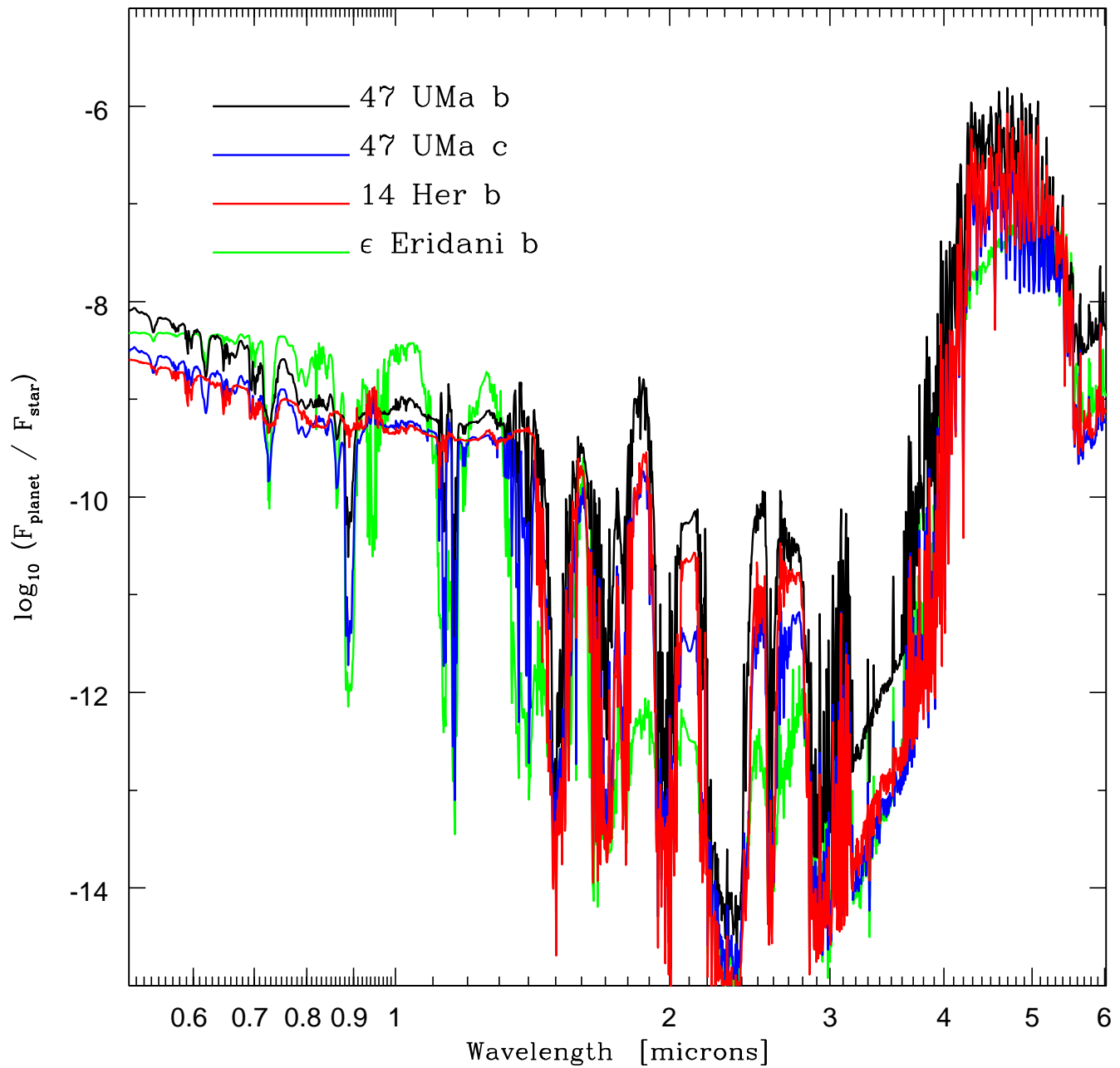


FIG. 11.— Same as Figs. 9 and 10, but for 47 UMa b, 47 UMa c, 14 Her b, and ϵ Eridani b. Refer to Fig. 9, Table 5, and the text for further details and discussion.